npj | computational materials

Article

Published in partnership with the Shanghai Institute of Ceramics of the Chinese Academy of Sciences

https://doi.org/10.1038/s41524-025-01760-w

Prediction of intrinsic multiferroicity and large valley polarization in a layered Janus material

Yulin Feng[1], Shaoxuan Qi[1], Yangyang Ren[1], Meng Liu[1], Na Liu[1], Meifeng Liu[1], Qing Yang[1] ✉ & Sheng Meng[2,3,4] ✉

Two-dimensional (2D) intrinsic multiferroics have attracted considerable attention for the next generation of advanced information technologies. Herein, we report that bilayer Janus FeSCl, a novel 2D system designed by substituting sulfur in monolayer 1T-$FeCl_2$, exhibits a giant spontaneous valley polarization and intrinsic magnetoelectric coupling. This Janus structure exhibits a ground-state bilayer structure that breaks space-inversion symmetry, enabling sliding ferroelectricity. Each monolayer displays robust intralayer ferromagnetic ordering, while the bilayer hosts interlayer antiferromagnetic alignment with opposing magnetic moments. Crucially, ferrovalley-mediated coupling links ferroelectric polarization and antiferromagnetic order, allowing electric-field-driven magnetic reversal. Notably, the direction of the net magnetic moment can be reversed through ferroelectric polarization switching, enabling nonvolatile control of the magnetism. The elucidated mechanisms are generalizable to diverse 2D material families, offering a universal framework for designing atomic-scale multiferroics. This work not only establishes foundational insights into 2D multiferroics but also advances the understanding of coupled charge-spin-valley physics in low-dimensional systems.

Multiferroics, which simultaneously exhibit multiple ferroic orders like ferroelectricity (spontaneous electric polarization), magnetism (spontaneous magnetization), and ferroelasticity (spontaneous strain), represent a frontier in condensed matter physics[1–4]. They provide a fertile platform for the development of next-generation devices that exploit couplings between these ferroic orders[5–7]. Among these, magnetoelectric multiferroics emerge as a standout example, in which the mutual control of magnetic states via electric fields (and vice versa) has potential applications in energy-efficient spintronics, non-volatile memory technologies, and quantum sensing[8–11]. However, the inherent lack of intrinsic magnetoelectric coupling in single-phase systems limits both fundamental investigations and practical applications. A groundbreaking solution emerges through ferrovalley materials, where spontaneous valley polarization serves as a pseudospin degree of freedom[12–15]. This framework transcends traditional multiferroic limitations, enabling valley pseudospin manipulation to drive magnetoelectric responses—a strategy especially potent in atomically thin layered systems.

The emergence of two-dimensional (2D) materials has fundamentally transformed material design through the utilization of van der Waals (vdW) engineering, a method that leverages weak interlayer interactions to precisely control quantum phenomena by manipulating interlayer stacking[16–19]. This flexibility has unveiled novel phenomena like sliding ferroelectricity, in which the polarization arises from stacking-induced symmetry-broken stacking of nonpolar monolayers like transition metal dichalcogenides and nitride bilayers[20–27]. Furthermore, by employing interlayer sliding and vdW engineering in 2D materials, theoretical studies have shown that stacking sequences can effectively modulate the electronic structure, resulting in layer-polarized anomalous Hall effects observed in bilayers such as $MnBi_2Te_4$, VSi_2P_4, and $VSiGeP_4$ bilayers[28–30]. Additionally, a theoretical study has revealed the coupling between ferroelectricity and antiferromagnetism via a ferrovalley in bilayer VS_2[31]. This mechanism has been validated in bilayer VSi_2N_4, demonstrating the magnetoelectric coupling mediated by valley polarization[32]. These advancements collectively highlight the versatility of 2D materials in integrating electronic, magnetic, and valleytronic functionalities, leading the way to a new frontier in quantum material design.

Recent advancements have unveiled monolayer 1T-$FeCl_2$, a synthetically realized 2D magnetic system. Experimental investigations have verified the intralayer ferromagnetic arrangement of monolayer $FeCl_2$, while its

[1]College of Physics and Electronic Science, Hubei Key Laboratory of Photoelectric Materials and Devices, Hubei Normal University, Huangshi, 435002, China. [2]Beijing National Laboratory for Condensed Matter Physics and Institute of Physics, Chinese Academy of Sciences, Beijing, 100190, China. [3]School of Physical Sciences, University of Chinese Academy of Sciences, Beijing, 100049, China. [4]Songshan Lake Materials Laboratory, Dongguan, 523808, China.
✉e-mail: yangqing@hbnu.edu.cn; smeng@iphy.ac.cn

bilayer counterpart exhibits interlayer antiferromagnetic coupling, as evidenced by spin-polarized scanning tunneling microscopy[33,34]. Theoretical studies additionally anticipate the presence of intrinsic multiferroicity in layered $FeCl_2$ systems, where ferroelectric (FE) polarization couples with both ferrovalley and interlayer antiferromagnetism[35,36]. Furthermore, Janus monolayers FeClF and FeClBr have been identified as ferromagnetic semiconductors with spontaneous valley polarization, stemming from the interplay between magnetic exchange interactions and spin-orbit coupling[37,38]. This interplay enables precise control over charge, spin, and valley degrees of freedom at the atomic level, establishing the 1T-FeXY material family as a paradigm for engineering 2D intrinsic multiferroics with magnetoelectric responses.

In this study, we present Janus-FeSCl, a novel stable layered material engineered from the monolayer 1T-$FeCl_2$, showcasing intrinsic multiferroicity by first-principles calculations. The monolayer Janus-FeSCl is identified as an intrinsic bipolar magnetic semiconductor with a pronounced valley polarization. Furthermore, our analysis reveals that the bilayer Janus-FeSCl exhibits ferroelectricity, interlayer A-type antiferromagnetism, and ferrovalley characteristics simultaneously. Notably, the ferrovalley facilitates a coupling between ferroelectricity and interlayer antiferromagnetism, allowing for nonvolatile electrical manipulation of the magnetism. This deterministic interplay positions Janus-FeSCl as a key candidate for exploring phenomena related to charge-spin-valley correlations and sets the stage for the development of atomically engineered multiferroic devices.

Results

Stability of monolayer Janus-FeSCl

Experimental and theoretical investigations have revealed that the majority of transition metal compounds tend to crystallize in single-layer T-phase or H-phase configurations. Recent advancements in synthesizing monolayer and few-layer 1T-$FeCl_2$ films have experimentally validated the 1T phase as the ground-state structure for monolayer $FeCl_2$[33,34]. Theoretical calculations have further established that 1T-$FeCl_2$ represents the energetically favorable state, whereas its 1H-phase counterpart is energetically less favorable by 0.17 eV per unit cell[35]. Inspired by the experimental synthesis of Janus-MoSSe achieved from MoS_2 by replacing one of the two S layers with Se atoms[39,40]. Figure 1a, b illustrates the optimized structure of the monolayer Janus-FeSCl, featuring a distinctive Cl-Fe-S sandwich configuration formed by substituting one Cl atomic layer in 1T-$FeCl_2$ with S atoms. Due to the broken vertical mirror symmetry, the space group of the monolayer Janus-FeSCl is identified as $P3m1$ (No. 156), which is lower than $P\bar{3}m1$ of the monolayer 1T-$FeCl_2$ (No. 164). The broken mirror symmetry in monolayer Janus-FeSCl endows the Janus structure with unique anisotropic piezoelectric properties: in-plane uniaxial strain simultaneously induces both in-plane and out-of-plane polarizations, whereas biaxial in-plane strain suppresses the in-plane piezoelectric effect while preserving vertical polarization.

The thermodynamic stability of Janus-FeSCl is meticulously evaluated through cohesive energy analysis, where the system's total energy is compared to the combined energies of its isolated constituent atoms, which is formulated as $E_c = E[\mathrm{Fe}] + E[\mathrm{S}] + E[\mathrm{Cl}] - E[\mathrm{FeSCl}]$. Our findings reveal that the cohesive energy of the monolayer Janus-FeSCl per unit cell stands at 2.48 eV/atom in the T-phase, showcasing robust atomic bonding compared to free atomic states. Moreover, the phonon dispersion spectra of the monolayer Janus-FeSCl were calculated using PHONOPY, as depicted in Fig. 1c. All phonon dispersion spectra along high-symmetry paths in the Brillouin zone exhibit strictly positive eigenfrequencies in all branches, confirming the dynamic stability of the structure. Additionally, an AIMD simulation of a $4 \times 4 \times 1$ supercell was performed to evaluate the thermal stability. As illustrated in Fig. 1d, there are neither bond breakages nor structural reconstructions in the simulation at 300 K after 5 ps, indicating its excellent thermal stability. The experimental synthesis of Janus-FeSCl is highly feasible, supported by precedents of Janus structures with mixed elemental groups[41,42]. Its favorable cohesive energy (2.48 eV/atom, comparable to $FeCl_2$), dynamical stability (no imaginary phonon modes), and thermal stability (intact structure at 300 K) further justify its realizability.

Electronic and magnetic properties of monolayer Janus-FeSCl

The magnetic properties of the monolayer Janus-FeSCl originate from the electronic configuration of Fe atoms, where partially filled $3d$ orbitals induce spin polarization. An isolated Fe atom with a valence electron configuration of $3d^6 4s^2$ undergoes charge redistribution in the monolayer structure, donating two electrons to sulfur and one electron to chlorine. This results in four d-electrons that fully populate two orbitals and partially occupy a third, generating a net magnetic moment of 1 μ_B per Fe atom. To identify the magnetic ground state of the monolayer Janus-FeSCl, three distinct configurations were systematically compared: ferromagnetic (FM)

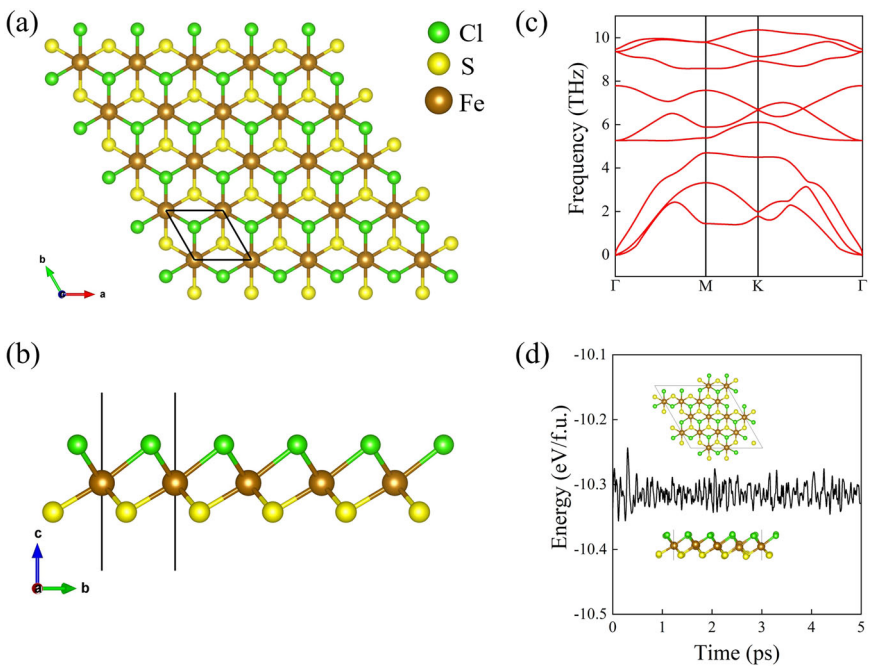

Fig. 1 | Structure and stability of monolayer Janus-FeSCl. a Top and **b** side views of the monolayer Janus-FeSCl; the green, yellow and brown spheres represent Cl, S, and Fe atoms, respectively. **c** The calculated phonon spectrum along the high-symmetry paths of the monolayer Janus-FeSCl. **d** AIMD simulation of the monolayer Janus-FeSCl at 300 K over 5 ps.

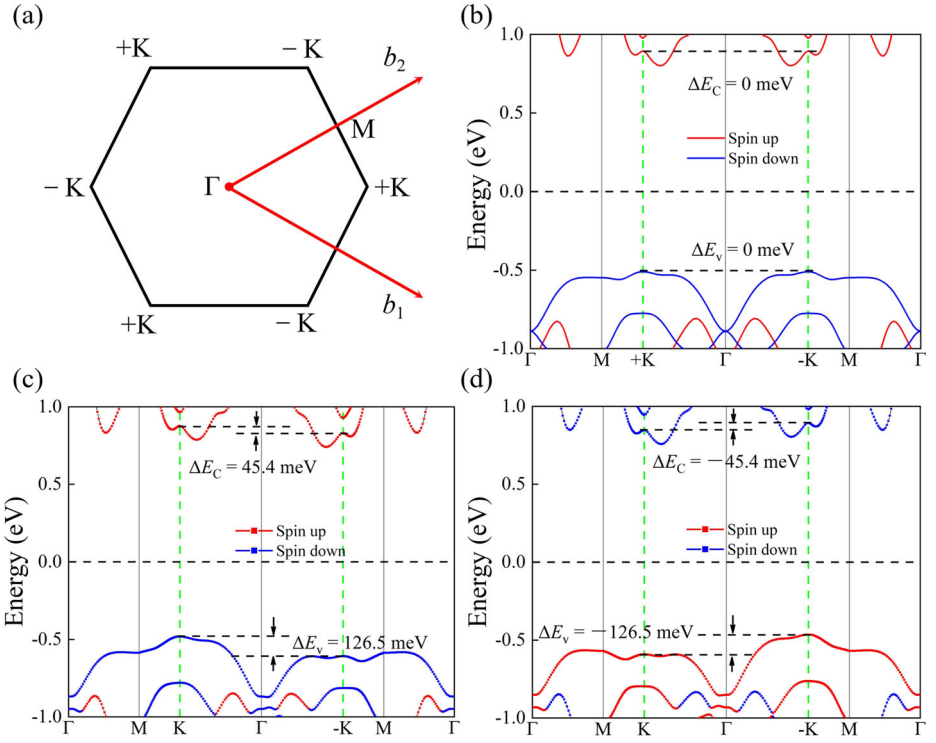

Fig. 2 | Giant valley polarization in monolayer Janus-FeSCl. a 2D Brillouin zone and high-symmetric points. **b** Band structure of monolayer Janus-FeSCl without SOC. Band structures of the monolayer Janus-FeSCl with SOC: **c** magnetic order is along the $+z$-axis and **d** the $-z$-axis.

configuration and two antiferromagnetic configurations (AFM1/AFM2), as shown in Fig. S1a–c. The results indicate that the monolayer Janus-FeSCl adopts a ferromagnetic ground state, whereas the AFM1 and AFM2 states exhibit energies higher than that of the FM state by 6.02 meV and 6.04 meV per unit cell, respectively. However, previous studies reveal that the magnetic anisotropy energy (MAE) plays an important role in the stability of magnetic order. Therefore, we investigate the MAE, defined as the energy difference MAE = $E_{001} - E_{100}$ between the magnetic moments along [001] and [100]. The MAE is 0.052 meV per unit cell, standing for the magnetization along the x-axis. For the monolayer Janus-FeSCl, a magnetic field ($H = -\frac{3}{4}\frac{K}{\mu_0 M}$) of 0.24 T is needed to tune the direction of magnetization from the x to z axis, which is one order of magnitude lower than the monolayer GdI_2 (3.58 T)[43].

In particular, the magnetic exchange mechanism can be analyzed through the Fe–S(Cl)–Fe super-exchange interaction based on the Goodenough-Kanamori-Anderson framework[44]. As illustrated in Fig. S2, the nearest Fe-Fe separation (~3.37 Å) effectively suppresses substantial direct exchange interactions. In the monolayer Janus-FeSCl, the S-mediated and Cl-mediated super-exchange interactions dominantly promote ferromagnetic coupling between adjacent Fe atoms, while the direct-exchange interaction is negligible. The bond angles in Fe–S–Fe (~95.3°) and Fe–Cl–Fe (~88.9°) closely approach the critical 90°, which activates 90° super-exchange interactions and inhibits 180° super-exchange interactions. These interactions strongly favor parallel spin alignment between adjacent Fe centers, thus stabilizing intralayer ferromagnetic alignment. The Curie temperature (T_C) is a critical parameter governing material applicability, particularly for spintronic and magnetic memory devices. Accordingly, we calculated T_C for both the pristine Janus-FeSCl monolayer and its structure under –5% biaxial strain (Fig. S3). The pristine system exhibits a T_C of ~72 K, surpassing that of monolayer CrI_3 (45 K)[19]. Notably, applying 5% compressive biaxial strain further enhances T_C to 138 K, demonstrating significant tunability under mechanical deformation.

The evolution of the electronic structure in the monolayer Janus-FeSCl with and without spin-orbit coupling (SOC) reveals unique valley physics enabled by the breaking of time-reversal and space-inversion symmetries. In contrast to the centrosymmetric monolayer 1T-$FeCl_2$, which suppresses valley polarization, the Janus configuration breaks space-inversion symmetry, leading to the emergence of spontaneous valley polarization. The spin-polarized band structure calculated using the PBE + U functional (without SOC) is shown in Fig. 2b along the high-symmetric k-paths outlined in Fig. 2a. The spin-up and spin-down channels exhibit significant splitting attributed to the magnetic exchange interactions. More intriguingly, our investigation reveals that the monolayer Janus-FeSCl acts as a bipolar magnetic semiconductor, wherein the valence band maximum and conduction band minimum are completely polarized (100%) in opposite spin directions.

Giant valley polarization in monolayer Janus-FeSCl

Notably, the valley degeneracy observed at the +K and −K in the spin-polarized bands ($\Delta E_{+K} = \Delta E_{-K}$) remains intact in the absence of SOC, as shown in Fig. 2b. The valley-dependent bands shift upwards or downwards after taking into account the SOC (see Fig. 2c, d). The underlying mechanisms of the spontaneous valley polarization of the monolayer Janus-FeSCl are ascribed to the magnetic exchange interactions and the SOC effects. Initially, the magnetic exchange interaction induces identical spin splitting at the +K and −K valleys in the absence of spin–orbit coupling. Subsequently, spin–orbit coupling introduces additional valley-dependent splitting, lifting the degeneracy between the valleys. This collective influence of exchange interactions and spin-orbit coupling results in the emergence of spontaneous valley polarization.

Upon considering spin-orbit coupling, the degeneracy at the +K and −K points in monolayer Janus-FeSCl is inherently broken, leading to a significant spontaneous valley polarization, as depicted in Fig. 2c, d. Specifically, the E^V_{+K} and E^V_{-K} evidently shift upward and downward, respectively, resulting in a large spontaneous valley ($\Delta E_V = E^V_{+K} - E^V_{-K}$) of 126.5 meV. More importantly, with a transition in magnetic order from spin up to spin down, the bands shift downward and upward, respectively, generating an opposite spontaneous valley of −126.5 meV and an opposite spin channel in the valence band maximum. This reversal in valley polarization upon spin-flip transitions highlights a direct connection between magnetic order and valley polarization. The magneto-valley locking observed validates ferrovalley functionality in Janus-FeSCl, enabling precise control through external magnetic fields.

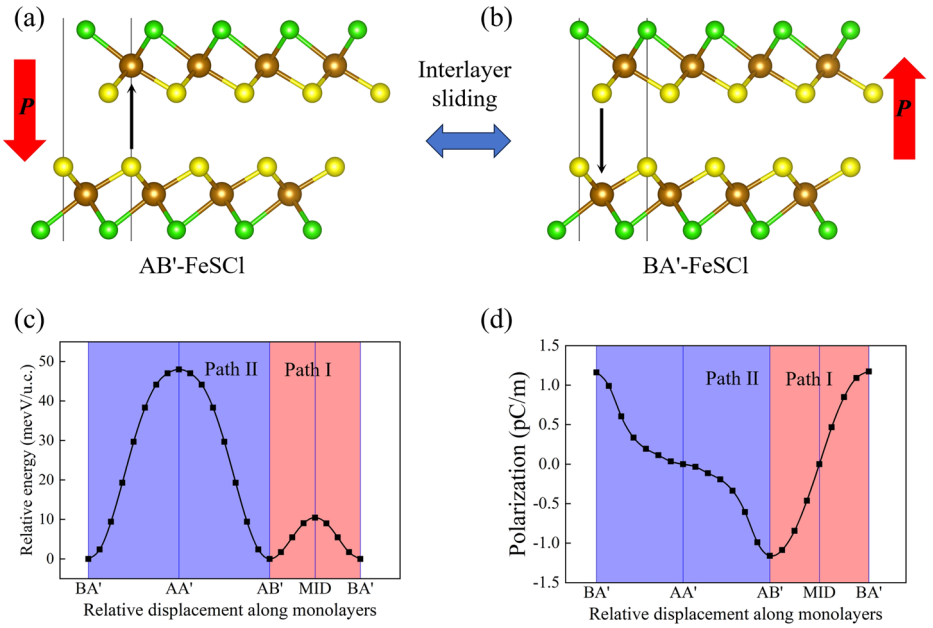

Fig. 3 | Sliding ferroelectricity in bilayer Janus-FeSCl. Geometry structures of **a** the bilayer AB'-FeSCl and **b** the bilayer BA'-FeSCl. Black arrows denote the directions of charge transfer. Red arrows denote the direction of FE polarization. **c** The energy barrier for Path I and Path II is displaced. **d** The dependence of vertical FE polarization from AB'-FeSCl to BA'-FeSCl on the sliding displacement along Path I and Path II. The red and blue shades denote Path I and Path II, respectively.

Intrinsic sliding ferroelectricity in bilayer Janus-FeSCl

This stability further enables versatile vdW engineering to construct bilayer architectures using the monolayer as a building block. As illustrated in Fig. S4a–c, we explore three distinct AB-stacking configurations, each maintaining interlayer space-inversion symmetry to prevent interlayer charge transfer. To break this symmetry, we introduce an additional operation involving a 180° rotation of the upper layer, resulting in anti-stacking (AB′-stacking) configurations (see Fig. S4d–f). The energy differences among these six stacking configurations were calculated, with the relative energies detailed in Table S1. Our results indicate that the AB′-stacking S–S configuration bilayer Janus-FeSCl (referred to as AB′-FeSCl) shown in Fig. S4f represents the most stable configuration with the lowest energy. In the AB′-FeSCl structure, the broken interlayer space-inversion symmetry induces uncompensated interlayer charge transfer, giving rise to out-of-plane FE polarization. Additionally, the magnetic moments distributed on these two single layers would be nonequivalent. These findings suggest the emergence of coexisting multiferroicity and magnetoelectric coupling in the bilayer system.

The geometry structure of the bilayer AB′-FeSCl configuration is illustrated in Fig. 3a, in which the S atoms in the lower layer lie below the Fe atoms in the upper layer, while the S atoms in the upper layer align directly above the hexagonal centers of the lower layer. Here, the misaligned stacking of the single layers and the distinct electronegativities of S and Fe atoms drive a strong net charge transfer from the lower layer to the upper layer. Consequently, the mirror symmetry along the z-axis of the bilayer AB′-FeSCl is broken, resulting in an out-of-plane FE polarization. Notably, this FE polarization can be reversed by interlayer sliding to the bilayer BA′-FeSCl configuration (see Fig. 3b), where the S atoms in the upper layer align over the Fe atoms in the lower layer, reversing the FE polarization to the $+z$-axis. Our analysis confirms the presence of out-of-plane FE polarization in AB′-FeSCl, showcasing bi-stable states equivalent to the binary “0” and “1” in nonvolatile memory applications.

In sliding ferroelectrics, the spontaneous out-of-plane FE polarization arises from a net interfacial charge transfer facilitated by weak vdW interactions. Figure 4a, b illustrates the charge density differences between the upper and lower layers of the AB′-FeSCl and BA′-FeSCl bilayers, validating the net charge transfer at the interface. The nonequivalence of charge distribution between the accumulation and depletion regions drives a net charge transfer between these single layers, giving rise to the out-of-plane FE polarization. The plane-averaged charge density difference along the z-axis in AB′-FeSCl reveals the negative charge accumulation in the upper layer, while the positive charge accumulation in the lower layer, reflecting net charge transfer from the lower layer to the upper layer and the spontaneous FE polarization along the $-z$-axis. Conversely, the net charge transfer occurs from the upper layer to the lower layer in BA′-FeSCl, leading to the spontaneous FE polarization along the $+z$-axis. The sliding ferroelectricity is further confirmed by analyzing the electrostatic potential. Figure 4c, d proposes that the positive (negative) discontinuity of the electrostatic potential difference is 55 meV (−55 meV) between the vacuum levels of the lower and upper layers, leading to the spontaneous out-of-plane FE polarization along the $-z$ ($+z$) axis in the AB′- (BA′-) stacking bilayer Janus-FeSCl. It is worth noting that the AB′- and BA′-stacking configurations possess the same energy as shown in Fig. 3c. These results confirm that the bilayer Janus-FeSCl exhibits intrinsic sliding ferroelectricity.

Ferroelectric phase transition in bilayer Janus-FeSCl

We investigate the FE phase transition in bilayer Janus-FeSCl by calculating the interlayer sliding pathways and energy landscapes using the NEB method, as shown in Fig. 3c, where the relative energy is considered for two layers sliding with respect to each other. The degenerate local minima in Fig. 3c correspond to the AB′- and BA′-stacking configurations, confirming the FE phase as a ground state. The distances from the AB′-FeSCl to the nearest and next nearest global minima BA′-FeSCl are $\sqrt{3}a/3$ and $2\sqrt{3}a/3$ Å, respectively, with a being the lattice constant. Due to the rotation symmetry C_{3z}, there are two pathways for transitioning from AB′-FeSCl to BA′-FeSCl through interlayer sliding, denoted as Path I and Path II in Fig. S5. For Path I, the AB′-FeSCl can be switched to BA′-FeSCl under the interlayer translation operation along $t[1/3, 2/3, 0]$, $t[-2/3, -1/3, 0]$ or $t[1/3, -1/3, 0]$. For Path II, the FE polarization switch can be achieved through interlayer sliding along three other equivalent directions, defined as $t[-2/3, -4/3, 0]$, $t[4/3, 2/3, 0]$, or $t[-2/3, 2/3, 0]$. The two intermediate states (see Fig. S6) exhibit non-polarity due to the presence of space-inversion symmetry.

The energy barriers for FE polarization switching along Path I and Path II are determined as 10.4 and 48.0 meV per unit cell, respectively, as depicted in Fig. 3c. Consequently, the markedly lower barrier of Path I indicates its favorability for FE switching in bilayer Janus-FeSCl. Notably, this value is smaller than that of bilayer VS_2 (~20.0 meV/u.c.)[31]. Furthermore, Fig. 3d illustrates that the FE polarizations for AB′-FeSCl and BA′-FeSCl are −1.16 pC/m and 1.16 pC/m, respectively, which are comparable in magnitude to bilayer h-BN (2.25 pC/m)[20,25]. It is evident that FE polarization is reversed

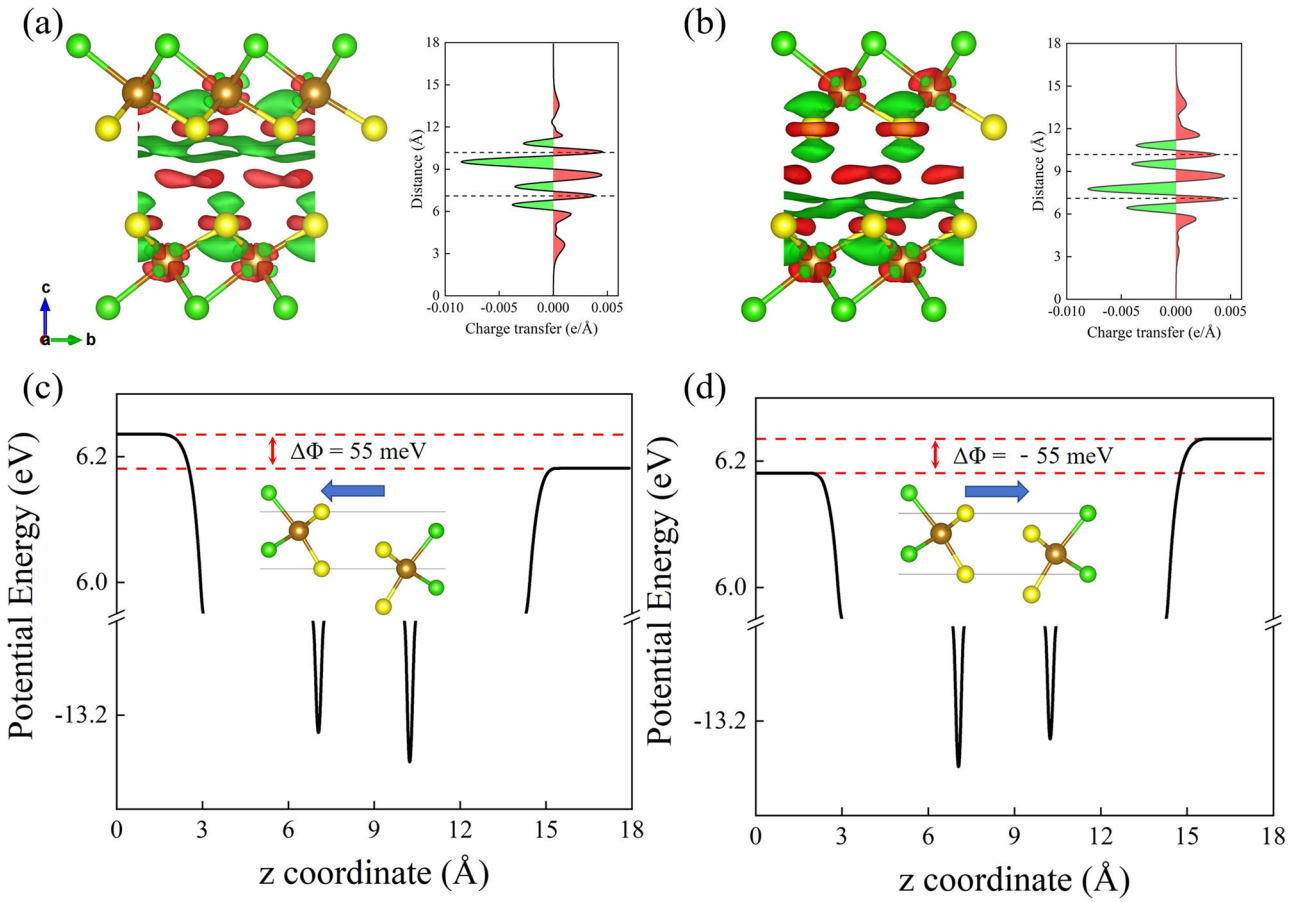

Fig. 4 | Origin of the out-of-plane ferroelectric polarization. Charge density differences and plane-averaged charge density differences along the *z*-axis of **a** the bilayer AB'-FeSCl and **b** the bilayer BA'-FeSCl, respectively. Green and red regions represent electron accumulation and depletion, respectively. The plane-averaged electrostatic potential of **c** the bilayer AB'-FeSCl and **d** the bilayer BA'-FeSCl, respectively. Blue arrows denote the directions of FE polarization.

along both Path I and Path II, with the intermediate states along these pathways showing no FE polarization. The equivalence of the charge accumulation and depletion regions in AA′-FeSCl and MID State configurations indicates no out-of-plane FE polarization (see Fig. S7a, b). Meanwhile, Fig. S7c, d illustrate that the electrostatic distributions in AA′-FeSCl and MID State remain the same between the upper and lower layers. These results further underscore space-inversion symmetry protection in AA′-FeSCl and MID State configurations, which rigorously suppress net FE polarization. We also reveal the A-type interlayer antiferromagnetism in bilayer Janus-FeSCl (see Note S2 and Fig. S8).

Magnetoelectric coupling and giant valley polarization in bilayer Janus-FeSCl

Electrically controlling magnetism is one of the key challenges of the next generation of information technology. 2D intrinsic multiferroics with magnetoelectric coupling are the ideal candidates to achieve electrically controlled magnetism. We have demonstrated that the bilayer Janus-FeSCl exemplifies such a platform, exhibiting coexisting sliding ferroelectricity and interlayer A-type antiferromagnetism, which synergistically enable magnetoelectric manipulation. While conventional ferroelectric bi-stability preserves electronic band degeneracy, the simultaneous breaking of time-reversal and space-inversion symmetries in bilayer Janus-FeSCl induces spontaneous valley polarization, as evidenced by first-principles calculations. The spin-polarized band structure was calculated via the PBE + U functional without SOC with the high-symmetry k-paths (see Fig. S9). Our results show that the bilayer Janus-FeSCl is an antiferromagnetic semiconductor, in which the valence band maximum (VBM) is located at the K point, while the conduction band minimum (CBM) is distributed along the Γ–K high-symmetry line. Without SOC, the CBM and VBM at the + K and −K points are degenerate. However, with the introduction of SOC, it lifts this valley degeneracy through spin-momentum locking, creating valley-specific energy offsets and enabling the spontaneous valley polarization. This interplay between spin-orbit interactions and symmetry-breaking establishes bilayer Janus-FeSCl as a prototype for nonvolatile devices, where magnetic and electric orders are coupled via ferrovalley.

To explore the interplay between intrinsic valley polarization and magnetoelectric coupling, we simulate four distinct FE/AFM configurations of the bilayer Janus-FeSCl, namely, $P\downarrow M\uparrow\downarrow$, $P\downarrow M\downarrow\uparrow$, $P\uparrow M\uparrow\downarrow$, and $P\uparrow M\downarrow\uparrow$ (see Fig. S10), where $P\uparrow$ ($P\downarrow$) represents the FE polarization directions oriented along the $+z$ ($-z$) axis, and $M\uparrow\downarrow$ represents the magnetic order of the lower (upper) layer along the positive (negative) direction of the z axis. Through our simulations, we find that all four configurations have degenerate energies, which provides a critical precondition for designing multistate memory devices with switchable ferroic orders. The electronic band structures of the FE bistable states with opposite FE polarization should also be indistinguishable. The spin-polarized band structures and Berry curvatures (BCs) under SOC for all configurations are systematically analyzed (see Fig. 5a–d). In two-dimensional honeycomb lattice systems, the extrema of the conduction and valence bands coincide at the same crystal momentum, localized at the corners of the hexagonal Brillouin zone. It is shown that the conduction band and valence bands at +K and −K points are nondegenerate, resulting in spontaneous valley polarization.

More importantly, we observe that the $P\downarrow M\uparrow\downarrow$ and $P\uparrow M\downarrow\uparrow$ configurations exhibit identical band structure as shown in Fig. 5a. Owing to the interaction of the interlayer ferrovalley, the splitting valleys at the bottom of

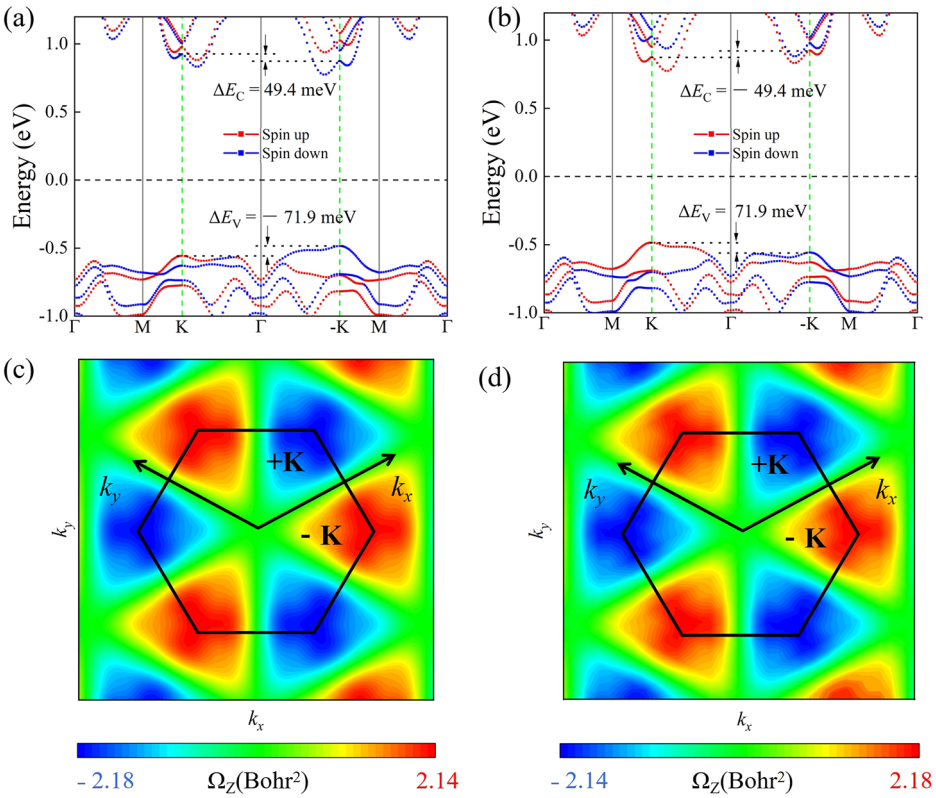

Fig. 5 | Magnetoelectric coupling and giant valley polarization in bilayer Janus-FeSCl. a The band structure **c** Berry curvatures with SOC of ferroelectric/antiferromagnetic configurations $P\downarrow M\uparrow\downarrow$ and $P\uparrow M\downarrow\uparrow$. **b** The band structure and **d** Berry curvatures with SOC of configurations $P\downarrow M\downarrow\uparrow$ and $P\uparrow M\uparrow\downarrow$. The red (blue) colors represent the bands of the spin projection in the positive (negative) directions of the *z*-axis (spin up or spin down).

the conduction band and the top of the valence band are not equal at +K and −K points. To quantify this phenomenon, the valley polarization is calculated as: $\Delta E_C = \Delta E_C^{+K} - \Delta E_C^{-K}, \Delta E_V = \Delta E_V^{+K} - \Delta E_V^{-K}$. For $P\downarrow M\uparrow\downarrow$ and $P\uparrow M\downarrow\uparrow$ configurations, the +K valley of the valence band is lower in energy than the −K valley, while the +K valley of the conduction band is higher in energy than the −K valley. This lifts the valley degeneracy, leading to the spontaneous valley polarization. Quantitatively, the valley polarization values are $\Delta E_C = 49.4$ meV, $\Delta E_V = -71.9$ meV for the $P\downarrow M\uparrow\downarrow$ and $P\uparrow M\downarrow\uparrow$ configurations, which are significantly higher than those of the bilayer $FeCl_2$. More intriguingly, if we just change the direction of the magnetic moment or the direction of the FE polarization to obtain the $P\uparrow M\uparrow\downarrow$ and $P\downarrow M\downarrow\uparrow$ configurations, the valley polarization values are $\Delta E_C = -49.4$ meV, $\Delta E_V = 71.9$ meV as shown in Fig. 5b, which are opposite to the case of the $P\downarrow M\uparrow\downarrow$ and $P\uparrow M\downarrow\uparrow$ configurations. We can clearly see that, for the $P\downarrow M\uparrow\downarrow$ and $P\uparrow M\downarrow\uparrow$ configurations, the spin-polarized structure of the VBM at +K(−K) point is spin up (spin down), while in the $P\uparrow M\uparrow\downarrow$ and $P\downarrow M\downarrow\uparrow$ configurations, the spin-polarized band structures are completely reversed. From the perspective of qualitative analysis of band structure, this provides indirect evidence that electrical control of the magnetism is achieved by ferrovalley coupling. Crucially, switching FE polarization necessitates a 180° flip in the magnetic moments of both layers to preserve the global band structure, demonstrating a coupling between ferroic orders through valley pseudospin.

The simultaneous breaking of space-inversion and time-reversal symmetries in the bilayer Janus-FeSCl generates pronounced non-zero Berry curvatures (BCs) localized at the +K and −K valleys, characterized by opposite signs and near-identical magnitudes (see Fig. 5c, d). Computed via the VASPBERRY code, the BCs for the $P\downarrow M\uparrow\downarrow$ and $P\uparrow M\downarrow\uparrow$ configurations manifest values of −2.18 $Bohr^2$ (+K) and +2.14 $Bohr^2$ (−K), respectively. Remarkably, reversing FE polarization or spin direction (e.g., $P\uparrow M\uparrow\downarrow$ and $P\downarrow M\downarrow\uparrow$) flips the magnitudes and directions of BCs to −2.14 $Bohr^2$ (+K) and +2.18 $Bohr^2$ (−K), preserving their antisymmetric relationships. Critically, this robust BC invariance under FE polarization switching necessitates a simultaneous 180° flip of magnetic moments in both layers, demonstrating magnetoelectric coupling mediated by ferrovalley. More intriguingly, for the $P\downarrow M\uparrow\downarrow$ configuration, the downward FE polarization creates an asymmetric magnetization distribution: Fe atoms in the upper layer exhibit a marginally larger magnetic moment than those in the lower layer, yielding a net magnetic moment of about -2×10^{-4} μ_B per unit cell. Strikingly, for the $P\uparrow M\uparrow\downarrow$ configuration, the net magnetic moment will be switched to 2×10^{-4} μ_B per unit with the reversal of the FE polarization, which is the direct evidence for the magnetoelectric coupling in bilayer Janus-FeSCl.

Discussion

In summary, based on first-principles density functional theory, we demonstrate that the bilayer Janus-FeSCl is an intrinsic 2D multiferroic material, unifying ferroelectricity, antiferromagnetism, and spontaneous valley polarization. We reveal that magnetoelectric coupling can be achieved in bilayer Janus-FeSCl by a ferrovalley to achieve electrical-controlled magnetism. We introduce a protocol to engineer four switchable ferroelectric/antiferromagnetic configurations, establishing a versatile platform for nonvolatile multistate memory and logic architectures. The emergence of spontaneous valley polarization and tunable sliding ferroic orders significantly broadens the design landscape of 2D sliding multiferroics, connecting structural adaptability with emergent quantum phenomena. This research sheds light on the underlying microscopic mechanisms governing the coexistence and reciprocal modulation of charge, spin, and valley degrees of freedom within atomically thin systems. By decoding the interplay between sliding mechanics and ferroic orders, our findings not only advance fundamental understanding of low-dimensional multiferroicity but also chart a pathway toward energy-efficient nanoelectronics.

Methods

Density functional theory calculations

All structural optimizations, total energy calculations, and electronic structure analyses are meticulously conducted utilizing the projected augmented-wave (PAW) method[45] within the Vienna ab initio simulation package (VASP)[46]. The exchange-correlation interactions are described by the generalized gradient approximation (GGA) of the

Perdew–Burke–Ernzerh (PBE)[47] with a plane-wave kinetic energy cutoff set at 500 eV. To obviate inter-slab interactions, a vacuum space of 15 Å is introduced. Atomic relaxations are conducted until convergence criteria for energy (10^{-6} eV) and force (0.01 eV/Å) are satisfied. The Grimme-D3 type of van der Waals (vdW) force correction[48] is included in our calculations, and the-centered k-mesh points of $15 \times 15 \times 1$ is adopted for structural optimization and energy calculations. According to previous work, the GGA + U method with an effective Hubbard parameter $U_{\text{eff}} = 4.0$ eV is applied to Fe-d orbitals exclusively during electronic structure calculations[49], albeit omitted from structural optimization. Phonon dispersion is computed via a supercell approach using density-functional perturbation theory (DFPT) as employed in the PHONOPY code[50]. Thermal stability is affirmed through ab initio molecular dynamics (AIMD) simulations at 300 K for 5 ps with a 1 fs timestep[51]. Ferroelectric (FE) polarization is determined via the Berry phase method[52,53], and energy barriers for polarization switching are computed employing the nudged elastic band (NEB) approach[54].

Calculations of Berry curvature

Berry curvature (BC) analysis is performed with the VASPBERRY toolkit. The BC is formally expressed as[55,56]:

$$\Omega_z(k) = -\sum_n \sum_{n \neq m} f_n(k) \frac{2\mathrm{Im}\langle \psi_{\mathrm{nk}} | \hat{\mathrm{v}}_{\mathrm{x}} | \psi_{\mathrm{mk}} \rangle \langle \psi_{\mathrm{nk}} | \hat{\mathrm{v}}_{\mathrm{y}} | \psi_{\mathrm{mk}} \rangle}{(E_{nk} - E_{mk})^2} \quad (1)$$

where $f_n(k)$ is the Fermi-Dirac distribution function with k being the electron wave vector; E_{nk} and E_{mk} are the eigenvalues of the Bloch wave functions ψ_{nk} and ψ_{mk}; $\hat{v}_x$ and $\hat{v}_y$ are velocity operators of the Dirac electrons; and n and m are the band indices.

Data availability

The data supporting the findings of this study are available within this article and its Supplementary Materials. Additional data that support the findings of this study are available from the corresponding author on reasonable requests. The central codes used in this paper are VASP. Detailed information related to the licence and user guide is available at https://www.vasp.at.

Received: 15 May 2025; Accepted: 31 July 2025;
Published online: 16 August 2025

References

1. Fiebig, M., Lottermoser, T., Meier, D. & Trassin, M. The evolution of multiferroics. *Nat. Rev. Mater.* **1**, 16046 (2016).
2. Eerenstein, W., Mathur, N. D. & Scott, J. F. Multiferroic and magnetoelectric materials. *Nature* **442**, 759 (2006).
3. Spaldin, N. A. & Ramesh, R. Advances in magnetoelectric multiferroics. *Nat. Mater.* **18**, 203 (2019).
4. Dong, S., Liu, J.-M., Cheong, S.-W. & Ren, Z. Multiferroic materials and magnetoelectric physics: symmetry, entanglement, excitation, and topology. *Adv. Phys.* **64**, 519 (2015).
5. Israel, C., Mathur, N. D. & Scott, J. F. A one-cent room-temperature magnetoelectric sensor. *Nat. Mater.* **7**, 93 (2008).
6. Dong, S., Xiang, H. & Dagotto, E. Magnetoelectricity in multiferroics: a theoretical perspective. *Natl Sci. Rev.* **6**, 629 (2019).
7. Scott, J. F. Applications of modern Ferroelectrics. *Science* **315**, 954 (2007).
8. Mostovoy, M. Multiferroics: different routes to magnetoelectric coupling. *npj Spintronics* **2**, 18 (2024).
9. Benedek, N. A. & Fennie, C. J. Hybrid improper ferroelectricity: a mechanism for controllable polarization-magnetization coupling. *Phys. Rev. Lett.* **106**, 107204 (2011).
10. Van Aken, B. B., Palstra, T. T. M., Filippetti, A. & Spaldin, N. A. The origin of ferroelectricity in magnetoelectric $YMnO_3$. *Nat. Mater.* **3**, 164 (2004).
11. Hu, J.-M., Duan, C.-G., Nan, C.-W. & Chen, L.-Q. Understanding and designing magnetoelectric heterostructures guided by computation: progresses, remaining questions, and perspectives. *NPJ Comput. Mater.* **3**, 18 (2017).
12. Tong, W.-Y., Gong, S.-J., Wan, X. & Duan, C.-G. Concepts of ferrovalley material and anomalous valley Hall effect. *Nat. Commun.* **7**, 13612 (2016).
13. Li, X., Cao, T., Niu, Q., Shi, J. & Feng, J. Coupling the valley degree of freedom to antiferromagnetic order. *Proc. Natl Acad. Sci. USA* **110**, 3738 (2013).
14. Lu, H.-Z., Yao, W., Xiao, D. & Shen, S.-Q. Intervalley scattering and localization behaviors of spin-valley coupled Dirac Fermions. *Phys. Rev. Lett.* **110**, 016806 (2013).
15. Xiao, D., Liu, G.-B., Feng, W., Xu, X. & Yao, W. Coupled spin and valley physics in monolayers of MoS_2 and other group-VI dichalcogenides. *Phys. Rev. Lett.* **108**, 196802 (2012).
16. Gong, C. et al. Discovery of intrinsic ferromagnetism in two-dimensional van der Waals crystals. *Nature* **546**, 265 (2017).
17. Yang, Q., Xiong, W., Zhu, L., Gao, G. & Wu, M. Chemically functionalized phosphorene: two-dimensional multiferroics with vertical polarization and mobile magnetism. *J. Am. Chem. Soc.* **139**, 11506 (2017).
18. Yang, Q. et al. Design of single-molecule multiferroics for efficient ultrahigh-density nonvolatile memories. *Adv. Sci.* **6**, 1801572 (2019).
19. Huang, B. et al. Layer-dependent ferromagnetism in a van der Waals crystal down to the monolayer limit. *Nature* **546**, 270 (2017).
20. Li, L. & Wu, M. Binary compound bilayer and multilayer with vertical polarizations: two-dimensional ferroelectrics, multiferroics, and nanogenerators. *ACS Nano* **11**, 6382 (2017).
21. Fei, Z. et al. Ferroelectric switching of a two-dimensional metal. *Nature* **560**, 336 (2018).
22. Yang, Q., Wu, M. & Li, J. Origin of two-dimensional vertical ferroelectricity in WTe_2 bilayer and multilayer. *J. Phys. Chem. Lett.* **9**, 7160 (2018).
23. Vizner Stern, M. et al. Interfacial ferroelectricity by van der Waals sliding. *Science* **372**, 1462 (2021).
24. Wang, X. et al. Van der Waals engineering of ferroelectric heterostructures for long-retention memory. *Nat. Commun.* **12**, 1109 (2021).
25. Yasuda, K., Wang, X., Watanabe, K., Taniguchi, T. & Jarillo-Herrero, P. Stacking-engineered ferroelectricity in bilayer boron nitride. *Science* **372**, 1458 (2021).
26. Wang, X. et al. Interfacial ferroelectricity in rhombohedral-stacked bilayer transition metal dichalcogenides. *Nat. Nanotechnol.* **17**, 367 (2022).
27. Yang, L., Ding, S., Gao, J. & Wu, M. Atypical sliding and Moiré ferroelectricity in pure multilayer graphene. *Phys. Rev. Lett.* **131**, 096801 (2023).
28. Peng, R. et al. Intrinsic layer-polarized anomalous Hall effect in bilayer $MnBi_2Te_4$. *Phys. Rev. B* **107**, 085411 (2023).
29. Zhang, T. et al. Layer-polarized anomalous Hall effects in valleytronic van der Waals bilayers. *Mater. Horiz.* **10**, 483 (2023).
30. Li, Y.-Q. et al. Magnetic and ferroelectric manipulation of valley physics in Janus piezoelectric materials. *Nano Lett.* **23**, 10013 (2023).
31. Liu, X., Pyatakov, A. P. & Ren, W. Magnetoelectric coupling in multiferroic bilayer VS_2. *Phys. Rev. Lett.* **125**, 247601 (2020).
32. Feng, Y. et al. van der Waals multiferroic tunnel junctions based on sliding multiferroic layered VSi_2N_4. *Phys. Rev. B* **109**, 085433 (2024).
33. Zhou, X. et al. Evidence of ferromagnetism and ultrafast dynamics of demagnetization in an epitaxial $FeCl_2$ monolayer. *ACS Nano* **18**, 10912 (2024).
34. Zhou, X. et al. Atomically thin 1T-$FeCl_2$ grown by molecular-beam epitaxy. *J. Phys. Chem. C* **124**, 9416 (2020).
35. Torun, E., Sahin, H., Singh, S. K. & Peeters, F. M. Stable half-metallic monolayers of $FeCl_2$. *Appl. Phys. Lett.* **106**, 192404 (2015).

36. Zhang, T., Xu, X., Huang, B., Dai, Y. & Ma, Y. 2D spontaneous valley polarization from inversion symmetric single-layer lattices. *NPJ Comput. Mater.* **8**, 64 (2022).
37. Guo, S.-D., Zhu, J.-X., Yin, M.-Y. & Liu, B.-G. Substantial electronic correlation effects on the electronic properties in a Janus FeClF monolayer. *Phys. Rev. B* **105**, 104416 (2022).
38. Li, R., Jiang, J., Mi, W. & Bai, H. Room temperature spontaneous valley polarization in two-dimensional FeClBr monolayer. *Nanoscale* **13**, 14807 (2021).
39. Lu, A.-Y. et al. Janus monolayers of transition metal dichalcogenides. *Nat. Nanotechnol.* **12**, 744 (2017).
40. Zhang, J. et al. Janus monolayer transition-metal dichalcogenides. *ACS Nano* **11**, 8192 (2017).
41. Antonatos, N. et al. Electrochemical exfoliation of janus-like bitei nanosheets for electrocatalytic nitrogen reduction. *ACS Appl. Nano Mater.* **4**, 590 (2021).
42. Liu, K. et al. Optimized synthesis and characterization of Janus RhSeCl with uniform anionic valences, nonlinear optical and optoelectronic properties. *Adv. Sci.* **2025**, e05279 (2025).
43. Xun, W. et al. Coexisting magnetism, ferroelectric, and ferrovalley multiferroic in stacking-dependent two-dimensional materials. *Nano Lett.* **24**, 3541 (2024).
44. Goodenough, J. B. Theory of the role of covalence in the perovskite-type manganites [La, *M*(II)]MnO3. *Phys. Rev.* **100**, 564 (1955).
45. Kohn, W. & Sham, L. J. Self-consistent equations including exchange and correlation effects. *Phys. Rev.* **140**, A1133 (1965).
46. Kresse, G. & Furthmüller, J. Efficient iterative schemes for ab initio total-energy calculations using a plane-wave basis set. *Phys. Rev. B* **54**, 11169 (1996).
47. Perdew, J. P., Burke, K. & Ernzerhof, M. Generalized gradient approximation made simple. *Phys. Rev. Lett.* **77**, 3865 (1996).
48. Grimme, S., Ehrlich, S. & Goerigk, L. Effect of the damping function in dispersion corrected density functional theory. *J. Comput. Chem.* **32**, 1456 (2011).
49. Liu, C., Zhao, G., Hu, T., Bellaiche, L. & Ren, W. Structural and magnetic properties of two-dimensional layered $BiFeO_3$ from first principles. *Phys. Rev. B* **103**, L081403 (2021).
50. Togo, A., Oba, F. & Tanaka, I. First-principles calculations of the ferroelastic transition between rutile-type and $CaCl_2$-type SiO_2 at high pressures. *Phys. Rev. B* **78**, 134106 (2008).
51. Barnett, R. N. & Landman, U. Born-Oppenheimer molecular-dynamics simulations of finite systems: structure and dynamics of H_2O_2. *Phys. Rev. B* **48**, 2081 (1993).
52. King-Smith, R. D. & Vanderbilt, D. Theory of polarization of crystalline solids. *Phys. Rev. B* **47**, 1651 (1993).
53. Shirodkar, S. N. & Waghmare, U. V. Emergence of ferroelectricity at a metal-semiconductor transition in a 1T monolayer of MoS_2. *Phys. Rev. Lett.* **112**, 157601 (2014).
54. Henkelman, G., Uberuaga, B. P. & Jónsson, H. A climbing image nudged elastic band method for finding saddle points and minimum energy paths. *J. Chem. Phys.* **113**, 9901 (2000).
55. Thouless, D. J., Kohmoto, M., Nightingale, M. P. & den Nijs, M. Quantized Hall conductance in a two-dimensional periodic potential. *Phys. Rev. Lett.* **49**, 405 (1982).
56. Kim, H.-J., Li, C., Feng, J., Cho, J.-H. & Zhang, Z. Competing magnetic orderings and tunable topological states in two-dimensional hexagonal organometallic lattices. *Phys. Rev. B* **93**, 041404 (2016).

Acknowledgements

We acknowledge partial financial support from the National Natural Science Foundation of China (Grants No. 12404267, No. 12404048, No. 12404104).

Author contributions

Q.Y., Y.F., and S.M. designed the idea of the research. Y.F. and S.Q. performed the first-principles calculations and wrote the manuscript. Q.Y., Y.F., S.M., S.Q., Y.R., M.L., N.L., and M.L. contributed to the general discussion, review and editing. Q.Y. supervised the research.

Competing interests

The authors declare no competing interests.

Additional information

Supplementary information The online version contains supplementary material available at https://doi.org/10.1038/s41524-025-01760-w.

Correspondence and requests for materials should be addressed to Qing Yang or Sheng Meng.